PCCP

ROYAL SOCIETY OF CHEMISTRY

PAPER

View Article Online
View Journal | View Issue

Check for updates

Cite this: *Phys. Chem. Chem. Phys.*, 2020, **22**, 8193

Effect of the supramolecular interactions on the nanostructure of halloysite/biopolymer hybrids: a comprehensive study by SANS, fluorescence correlation spectroscopy and electric birefringence†

Giuseppe Cavallaro, *[abc] Leonardo Chiappisi, [cd] Michael Gradzielski [c] and Giuseppe Lazzara [ab]

The structural properties of halloysite/biopolymer aqueous mixtures were firstly investigated by means of combining different techniques, including small-angle neutron scattering (SANS), electric birefringence (EBR) and fluorescence correlation spectroscopy (FCS). Among the biopolymers, non-ionic hydroxypropylcellulose and polyelectrolytes (anionic alginate and cationic chitosan) were selected. On this basis, the specific supramolecular interactions were correlated to the structural behavior of the halloysite/biopolymer mixtures. SANS data were analyzed in order to investigate the influence of the biopolymer adsorption on the halloysite gyration radius. In addition, a morphological description of the biopolymer-coated halloysite nanotubes (HNTs) was obtained by the simulation of SANS curves. EBR experiments evidenced that the orientation dynamics of the nanotubes in the electric field is influenced by the specific interactions with the polymers. Namely, both variations of the polymer charge and/or wrapping mechanisms strongly affected the HNT alignment process and, consequently, the rotational mobility of the nanotubes. FCS measurements with fluorescently labeled biopolymers allowed us to study the aqueous dynamic behavior of ionic biopolymers after their adsorption onto the HNT surfaces. The combination of EBR and FCS results revealed that the adsorption process reduces the mobility in water of both components. These effects are strongly enhanced by HNT/polyelectrolyte electrostatic interactions and wrapping processes occurring in the halloysite/chitosan mixture. The attained findings can be useful for designing halloysite/polymer hybrids with controlled structural properties.

Received 25th February 2020,
Accepted 16th March 2020

DOI: 10.1039/d0cp01076f

rsc.li/pccp

Open Access Article. Published on 16 2563. Downloaded on 31/1/2569 9:59:45.
This article is licensed under a Creative Commons Attribution 3.0 Unported Licence.

Introduction

In the last decades, supramolecular hybrids based on inorganic nanoparticles and organic macromolecules have attracted great interest as a consequence of their potential applications in several technological fields, including packaging,[1,2] catalysis,[3–8] pharmaceutics,[8–14] and remediation.[15–19] As evidenced in a recent review,[20] the adsorption of sustainable polymers can confer functional properties to the nanoparticles depending on their peculiar nanoarchitecture. It was proved that the modification of carbon[21] and boron[22] nanotubes with poly(*N*-isopropylacrylamide) (PNIPAAm) generates hybrid molecular nanorods with assembly/disassembly behaviors in response to temperature variations. Recently, thermo-sensitive nanocarriers were obtained by

[a] *Dipartimento di Fisica e Chimica, Università degli Studi di Palermo, Viale delle Scienze pad 17, 90128 Palermo, Italy. E-mail: giuseppe.cavallaro@unipa.it; Tel: +39 09123897962*
[b] *Consorzio Interuniversitario Nazionale per la Scienza e Tecnologia dei Materiali, INSTM, Via G. Giusti, 9, I-50121 Firenze, Italy*
[c] *Stranski Laboratorium für Physikalische und Theoretische Chemie, Institut für Chemie, Technische Universität Berlin, Straße des 17. Juni 124, Sekr. TC 7, 10623 Berlin, Germany*
[d] *LSS Group, Institut Laue-Langevin, 6 rue Jules Horowitz BP 156, F-38042 Grenoble, Cedex 9, France*

† Electronic supplementary information (ESI) available: Density and scattering length density of solvent, biopolymers and HNT used in the SANS data analysis; scattering length density of the nanotube shell for HNT/biopolymer hybrids based on their composition from Guinier analysis; fitting parameters obtained by the analysis of FCS curves for DTAF/alginate and HNT/DTAF/alginate suspensions using the triplet sate model. SEM images of halloysite nanotubes. Fitting analysis (with the corresponding residuals) of the decay of the electric birefringence as a function of time after the termination of the voltage for aqueous dispersion of mass ratio HPC/HNT = 0.1. The rotational diffusion coefficient and the corresponding length determined by the analysis of EBR data as a function of the biopolymer/HNT mass ratio. Details on the calculation of the length from rotational diffusion coefficient. Details on the preparation of fluorescently labelled biopolymers (DTAF/alginate and FITC/chitosan). Details on the calculation of the number density and the volume of halloysite nanotubes. Details on the determination of the HNT/biopolymer volume ratio of the coated nanotubes. See DOI: 10.1039/d0cp01076f

Open Access Article. Published on 16 2563. Downloaded on 31/1/2569 9:59:45.
This article is licensed under a Creative Commons Attribution 3.0 Unported Licence.

supramolecular functionalization of halloysite with oppositely charged PNIPAAm polymers, such as amine-terminated PNIPAAM and PNIPAAM/methacrylic acid copolymer.[23] Electrostatic interactions were successfully exploited to fabricate pH-sensitive drug delivery hybrids based on LAPONITE® nanodisks and poly(ethylene glycol)–poly(lactic acid) diblock copolymer.[24] Efficient nanocarriers for drugs were prepared by the adsorption of alginate onto calcium carbonate[25] and silica nanoparticles.[26]

Among inorganic nanoparticles, halloysite clay nanotubes (HNTs) are suitable for the preparation of smart nanohybrids because of their peculiar surface properties in terms of chemical composition and electrical charge.[27] In particular, the chemical composition of the HNT internal surface is based on alumina, while the external shell is formed by silica. As a consequence of the different acid–base equilibria of alumina and silica groups, the HNT inner and external surfaces are positively and negatively charged, respectively, within an extended pH interval and, in addition, the charge conditions can be tuned by pH.[28] Rheological measurements evidenced that HNT aqueous suspensions can form a lyotropic liquid crystalline phase depending on the pH conditions.[29] The HNT dispersions exhibited stronger shear-thinning behavior by the addition of microcrystalline cellulose.[30] The HNT surfaces can be selectively modified by ionic molecules through electrostatic interactions.[20] The adsorption of cationic alkyltrimethylbromides onto the halloysite outer surface allows fabrication of inorganic reverse micelles,[31] which were used to synthesize alginate-based nanohydrogels within the HNT lumen.[32] The attractions between anionic surfactants and the positively charged internal surface generated functionalized nanotubes with a hydrophobic cavity.[33,34] As evidenced by SANS studies,[33] the structural organization of the adsorbed surfactants affects the hydrophobization degree of the modified halloysite lumen. The immobilization of several enzymes within the HNT lumen was controlled by pH conditions, which influence the electrostatic forces occurring between proteins and halloysite surfaces.[35]

The literature[36] reports that the addition of ionic and non-ionic macromolecules represents an efficient tool to control the HNT colloidal stability in aqueous solvent. Halloysite aqueous dispersions were stabilized by the adsorption of non-ionic biopolymers (amylose[37] and cellulose ethers[36]) because of their wrapping around the nanotubes generating a steric barrier toward HNT aggregation in water. The presence of anionic polymers (pectin[36] and poly(styrene)sulfonate[38,39]) induced an increase of the HNT aqueous colloidal stability as a consequence of electrostatic interactions, which alter the halloysite surface charge. Specifically, the selective adsorption of anionic polymers induced a neutralization of the positively charged inner surface generating an increase of the HNT negative charge.[36,39] Specific interactions between biopolymers and halloysite surfaces affect the HNT efficacy as nanocontainers for drugs.[36] In this regard, nanotubes with enhanced adsorption capacity and sustained-release performance towards ibuprofen were obtained by the self-assembly of chitosan and alginate onto halloysite surfaces.[40] Biopolymer/HNT layered tablets for diclofenac were successfully prepared by exploiting the electrostatic interactions between polyelectrolytes and halloysite.[41] However, despite a number of studies existing on HNT/polymer hybrid systems, still, many questions in that area are open, especially with respect to their dispersion stability in aqueous solution, which is an important aspect for most of their potential applications.

Accordingly, studies on the structure and dynamics of polymer/HNT hybrids in water could be crucial to understand the stabilization mechanism controlling the aqueous colloidal stability of the nanotubes. In this work, we investigated the structural behavior of aqueous mixtures based on halloysite and biopolymers with different charges, including non-ionic hydroxypropylcellulose and biopolyelectrolytes (anionic alginate and cationic chitosan), in order to explore the influence of the specific supramolecular interactions on the nanoarchitecture of the HNT/biopolymer hybrids. These investigations were conducted by using a comprehensive approach based on combining different methods (small-angle neutron scattering, fluorescence correlation spectroscopy and electric birefringence) not employed before together for the characterization of polymer/HNT hybrids, with the aim of gaining an improved understanding of their interactions and structures and the resulting stability in aqueous solutions.

Giuseppe Cavallaro

Dr Giuseppe Cavallaro is an Assitant Professor at the Department of Physics and Chemistry, University of Palermo, Italy. He was a Research Associate at Institute of Micromanufacturing, Lousiana Tech Univesity, (USA) and at Institut für Chemie, Technische Universität Berlin (Germany). His research activities focus on nanoclays and polymer/nanoparticle interactions. He is the author of 77 pubblications in peer-reviewed international journals. Based on Scopus source, his h-index is 31.

Materials and methods

Chemicals

Hydroxypropyl cellulose (HPC; average molecular weight = 80 kg mol^{-1}), sodium alginate (average molecular weight = 90 kg mol^{-1}), chitosan (deacetylation degree = 75–85%, average molecular weight = 120 kg mol^{-1}), fluorescein isothiocyanate (FITC), 5-[(4,6-dichlorotriazin-2-yl)amino]fluorescein (DTAF), phosphate-buffered saline (PBS), sodium bicarbonate ($NaHCO_3$), sodium hydroxide (NaOH) and glacial acetic are Sigma products. Halloysite (HNT, purity $\geq$99.5%) from Matauri Bay was provided by Imerys. SEM images of HNTs are presented in the ESI.† All the chemicals were used without further purification. Water was of Millipore grade. D_2O was purchased from Eurisotop in 99.9% isotopic purity.

This journal is © the Owner Societies 2020

Open Access Article. Published on 16 2563. Downloaded on 31/1/2569 9:59:45.
This article is licensed under a Creative Commons Attribution 3.0 Unported Licence.

Preparation of HNT/biopolymer dispersions

HNT/biopolymer dispersions in aqueous solvents were prepared as reported elsewhere.[36] Firstly, stable aqueous solutions of each polymer were obtained by magnetically stirring at 25 °C for 3 h. Chitosan was solubilized in acidic solvent (pH = 4.5) because of its low solubility under neutral conditions. The pH of the aqueous solvent was adjusted by adding glacial acetic acid. The final concentration of acetic acid was set at 5 g dm^{-3} (0.083 mol dm^{-3}). Then, HNT/biopolymer dispersions with various compositions were obtained by direct addition of appropriate amounts of halloysite powder into the polymer solutions. The HNT/biopolymer mixtures were homogenized by ultrasonication for 10 min and subsequent magnetic stirring at 25 °C for 24 h.

Small-angle neutron scattering (SANS)

SANS measurements were carried out at Institut Laue-Langevin (ILL), Grenoble (France), on the instrument D11.[42] The experiments were conducted at four different configurations with sample-to-detector (and collimation in parenthesis) distances of 1.5 m (8 m), 8 m (8 m), and 34 m (34 m), using a wavelength λ of 6.0 Å (fwhm of 10%) and 39 m (40.5 m) with λ = 13.0 Å and fwhm of 10%. Based on these experimental conditions, the investigated scattering vector ($q = 4\pi\sin(\theta/2)/\lambda$, θ being the scattering angle) ranged between 0.007 and 4.20 nm^{-1}. The two-dimensional patterns were corrected for the detector efficiency using the scattering of a 1 mm H_2O sample and for the dark current signal; the contribution from the empty cell was subtracted; and finally, the patterns were radially averaged as all samples were scattering isotropically. Data reduction was performed with LAMP,[43] while SASfit 0.94.8 software[44] was used for the analysis of SANS curves in absolute scale. The experiments were performed in full contrast conditions (D_2O as solvent) on halloysite/biopolymer dispersions. Similar to our previous work on pristine halloysites,[45] the HNT concentration was set at 80 g dm^{-3}. Raw and reduced SANS data are available free of charge at doi:10.5291/ILL-DATA.9-12-473.[42]

Electric birefringence (EBR)

EBR experiments were conducted using rectangular pulses of the electric field (1.25×10^5 V m^{-1}) generated by a Cober high power pulse generator (Model 606). The pulse length was fixed at 2.5 ms. The quartz cuvettes were illuminated with a He/Ne laser (633 nm), and the signal was detected by a photomultiplier and recorded on a Datalab transient recorder, DL 920. EBR measurements were performed on halloysite/biopolymer aqueous dispersions with various compositions. The HNT concentration was fixed at 0.15 g dm^{-3}, while the halloysite/biopolymer mass ratio was systematically changed from 0 to 0.95. It should be noted that EBR experiments for halloysite/chitosan mixtures were conducted in acidic solvent (pH = 4.5, concentration of acetic acid of 5 g dm^{-3}). All mixtures were thermostated at 25 °C.

Fluorescence correlation spectroscopy (FCS)

FCS experiments were conducted by using a Leica TCS SMD FCS system with hardware and software for FCS from PicoQuant (Berlin, Germany) integrated into a high-end confocal system, a Leica TCS SP5 II instrument. The calibration of the confocal volume (0.135 fL) was performed by measuring the characteristic time of Rhodamine 6G (5×10^{-9} mol dm^{-3}) in water with a known diffusion coefficient of 4.0×10^{-10} m^2 s^{-1}.[46] An argon laser (λ = 488 nm) was employed for the excitation of the fluorescent probes. Alginate was fluorescently labeled by using 5-[(4,6-dichlorotriazin-2-yl)amino]fluorescein (DTAF),[47,48] while fluorescein isothiocyanate (FITC) was selected as the fluorescent probe for chitosan.[49] Details on the preparation of fluorescently labeled polymers (DTAF/alginate and FITC/chitosan) are reported in the ESI.† FCS measurements were conducted on the HNT/labeled biopolymer aqueous mixtures and on the aqueous solutions of the pure labeled biopolymers. The concentrations of the labeled polymers were set at 0.05 and 0.1 mg dm^{-3} for FITC/chitosan and DTAF/alginate, respectively. The overall concentrations of the polymers were fixed at 5 and 10 g dm^{-3} for chitosan and alginate, respectively. We selected 50 and 100 g dm^{-3} as halloysite concentrations for chitosan- and alginate-based mixtures, respectively. On this basis, the mass ratio between HNT and the labeled biopolymer was fixed at $1:10^{-4}$. On the other hand, the HNT/biopolymer mass ratio was 10 : 1.

Scanning electron microscopy (SEM)

The surface morphology of halloysite nanotubes was investigated using a microscope, ESEM FEI QUANTA 200F. Before each experiment, the surface of the sample was coated with gold in argon by means of an Edwards Sputter Coater S150A to avoid charging under the electron beam. The measurements were carried out in high vacuum mode ($< 6 \times 10^{-4}$ Pa) for simultaneous secondary electrons; the energy of the beam was 25 kV and the working distance was 10 mm.

Results and discussion

SANS data analysis: structural characterization of HNT/biopolymer hybrids

Fig. 1 shows the scattering curves in full contrast for HNT and HNT/biopolymer dispersions with a mass ratio of biopolymer/HNT of 0.1.

As observed for pure halloysite from different sources,[45] SANS curves of the HNT/biopolymer mixtures did not evidence any oscillations, in agreement with the large polydispersity of the HNT radii. Similar observations were detected for HNT/surfactant systems.[33]

According to the literature,[50,51] two different Guinier regions can be considered for elongated particles, such as rigid rods. Within the low q Guinier interval, the scattered intensity of elongated objects varies as

$$I(q) = I(0) \times \exp\left(-\frac{R_g^2 q^2}{3}\right) \quad (1)$$

where $I(0)$ is the scattering intensity at the limit $q \to 0$, while R_g is the gyration radius of the whole particle, which is related to the length (L) and the radius (R) of the scattered rod by the following relation

$$R_g^2 = (L^2)/12 + (R^2)/2 \quad (2)$$

Open Access Article. Published on 16 2563. Downloaded on 31/1/2569 9:59:45.
This article is licensed under a Creative Commons Attribution 3.0 Unported Licence.

On this basis, we calculated that the theoretical R_g of halloysite nanotubes is 294 nm by taking into account their average sizes in terms of length (1000 nm) and external radius (80 nm).[45]

According to eqn (1), $\ln(I(q))$ *vs.* q^2 plots describe linear trends allowing us to determine R_g and $I(0)$ from their slopes and their intercepts, respectively. SANS data at small angles ($0.007\ \text{nm}^{-1} \leq q \leq 0.009\ \text{nm}^{-1}$) were analyzed by eqn (1). As displayed in Fig. 2, $\ln(I(q))$ was linearly dependent on q^2 for all of the investigated dispersions. Table 1 collects the R_g and $I(0)$ data obtained from the Guinier analysis of SANS curves.

In addition, the Guinier analysis for elongated particles can be conducted in the intermediate q range, where the dependence of the scattered intensity on the radial gyration radius is expressed as

$$q \cdot I(q) = I^*(0) \times \exp\left(-\frac{R_g^2 q^2}{2}\right) \quad (3)$$

where $I^*(0)$ is the prefactor and ${R_g}^2 = R^2/2$ and, thus, we can state that R_g determined from the intermediate q region is related only to the cross section of the rod.[52] Accordingly, we calculated $R_g = 53$ nm for cylinders with $R = 80$ nm, which is the average outer radius of halloysite nanotubes.[45] By taking into account both the inner and the outer radii of halloysite (80 and 15 nm, respectively),[45] we estimated $R_g = 57$ nm for the cross section of the hollow nanotube.

It should be noted that eqn (3) is valid for $q \cdot R_g \approx 1$, which indicates that q values between 0.015 and 0.02 nm^{-1} represent the proper intermediate q range for scattered halloysite. As expected by eqn (3), $\ln(q \cdot I(q))$ *vs.* q^2 plots within the intermediate q range (Fig. 2) were successfully fitted by linear equations that provided the corresponding R_g and $I^*(0)$ values (Table 1).

From the Guinier linear analysis for elongated objects, we find that the halloysite gyration radii are hardly affected by the adsorption of both anionic alginate and cationic chitosan (Table 1).

Regarding $I(0)$, the HNT/biopolymer composites showed slightly larger values with respect to that of pure HNT (Table 1) due to the polymer adsorption onto the halloysite surfaces.

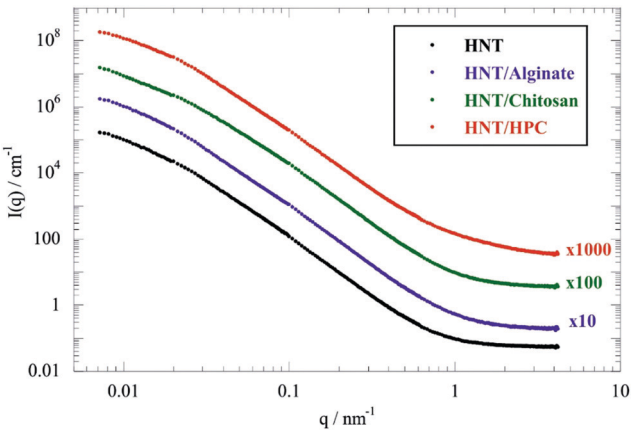

Fig. 1 SANS intensity as a function of q, the magnitude of the scattering vector, for HNT/chitosan, HNT/alginate, HNT/HPC and HNT dispersions in D_2O. The HNT concentration and the HNT/biopolymer mass ratio were 80 g dm^{-3} and 10, respectively.

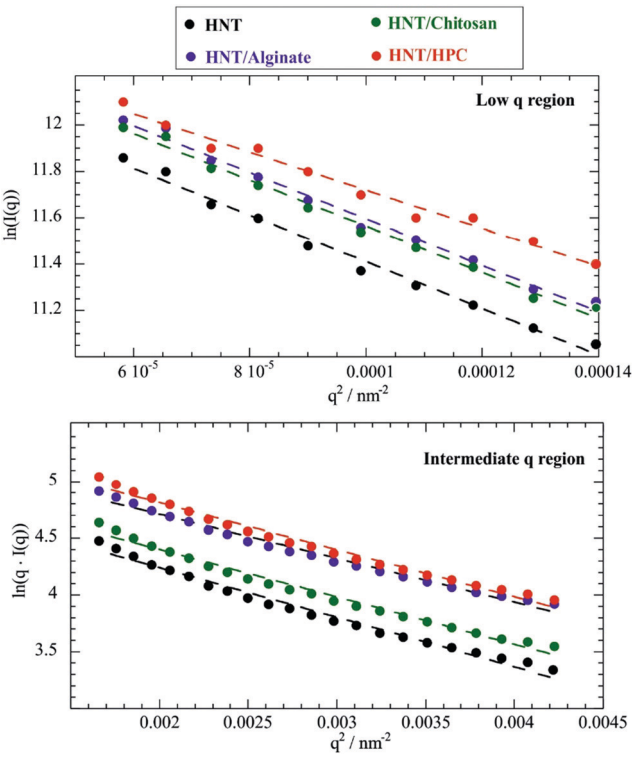

Fig. 2 Guinier plots for HNT/chitosan, HNT/alginate, HNT/HPC and HNT dispersions in D_2O within the low ($0.007\ \text{nm}^{-1} \leq q \leq 0.009\ \text{nm}^{-1}$) and the intermediate ($0.015\ \text{nm}^{-1} \leq q \leq 0.02\ \text{nm}^{-1}$) regions. The low q Guinier plot is $\ln(I(q))$ *vs.* q^2 (top), while the intermediate q Guinier plot is $\ln(q \cdot I(q))$ *vs.* q^2 (bottom). Dashed lines represent the fitting according to eqn (1) and (3).

As reported for silica/polyelectrolytes systems,[53] the actual amount of biopolymer adsorbed onto the nanotubes can be calculated from $I(0)$ values, which are related to the density (^1N) and the volume (V) of the nanoparticles by the following equation

$$I(0) = {}^1N \cdot V^2 \cdot \Delta\text{SLD}^2 \cdot S(0) \quad (4)$$

where $S(0)$ is the structure factor at $q \to 0$, whereas ΔSLD is the difference between the scattering length density of the nanoparticle ($\text{SLD}_{\text{nanoparticle}}$) and that of the solvent ($\text{SLD}_{\text{solvent}}$). ^1N is the number density of HNT and was determined by the concentration and HNT geometry considering the corresponding polydispersity. Based on eqn (4), we calculated $I(0) = 27.6 \times 10^5\ \text{cm}^{-1}$ for the pure HNT solution, which is close to the experimental result (Table 1). Details on the calculation of the number density (^1N) and the volume (V) of HNT are presented in the ESI.†

As concerns the biopolymer coated nanotubes, the volume ($V_{\text{HNT/Biop}}$) and the scattering length density ($\text{SLD}_{\text{HNT/Biop}}$) of the hybrid nanoparticles can be expressed as

$$V_{\text{HNT/Biop}} = V_{\text{HNT}} + \chi \cdot (\phi_{\text{Biop}}/{}^1N_{\text{HNT}}) \quad (5)$$

$$\text{SLD}_{\text{HNT/Biop}} = (\text{SLD}_{\text{HNT}} \cdot V_{\text{HNT}} + \text{SLD}_{\text{Biop}} \cdot \chi \cdot (\phi_{\text{Biop}}/{}^1N_{\text{HNT}}))/ (V_{\text{HNT}} + \chi \cdot (\phi_{\text{Biop}}/{}^1N_{\text{HNT}})) \quad (6)$$

This journal is © the Owner Societies 2020

Table 1 Fitting parameters obtained by the Guinier analysis of SANS data

	$I(0)/10^5$ cm^{-1} (from low q region)	R_g/nm (from low q region)	$I^*(0)$/cm^{-1} (from intermediate q region)	R_g/nm (from intermediate q region)
HNT	27.4 ± 1.0	223 ± 18	166 ± 2	41 ± 5
HNT/alginate	31.7 ± 1.1	222 ± 19	240 ± 2	39 ± 5
HNT/chitosan	30.8 ± 1.1	226 ± 21	187 ± 2	40 ± 4
HNT/HPC	30.5 ± 1.2	209 ± 20	281 ± 3	40 ± 5

Table 2 Quantitative adsorption parameters for HNT/biopolymer hybrids at a biopolymer/HNT mass ratio of 0.1, as determined by the Guinier analysis of SANS data in the low q range

	χ	$R_{V(Biop/HNT)}$	Z/mg m^{-2}
HNT/alginate	2.97×10^{-2}	7.56×10^{-3}	3.44 ± 0.06
HNT/chitosan	1.78×10^{-2}	4.21×10^{-3}	2.19 ± 0.07
HNT/HPC	9.61×10^{-3}	2.38×10^{-3}	1.48 ± 0.03

where ϕ_{Biop} and V_{HNT} are the total volume fraction of biopolymer and the volume of uncoated HNT, while χ corresponds to the fraction of biopolymer adsorbed onto halloysite with respect to all the biopolymer in the dispersion.

Assuming $S(0) = 1$, the numerical solution of eqn (2)–(4) allowed us to estimate χ from the $I(0)$ values. Based on the calculated χ values (Table 2), we calculated the biopolymer/HNT volume ratio ($R_{V(Biop/HNT)}$) of the coated nanotubes, as detailed in the ESI.†

The biopolymer surface coverage (Z) onto the HNTs was calculated by using the $R_{V(HNT/Biop)}$ values and taking into account the specific surface area (SSA) of halloysite (28.3 m^2 g^{-1})[45] through the following equation

$$Z = \rho_{Biop}/(\rho_{HNT}\cdot SSA_{HNT}\cdot R_{V(Biop/HNT)}) = C_{HNT}/(C_{Biop}\cdot\chi\cdot SSA_{HNT}) \quad (7)$$

As evidenced in Table 2, we observed larger Z values for the ionic biopolymers compared to that of HPC indicating that the electrostatic interactions play a crucial role in the formation of complex systems based on halloysite. For chitosan and alginate, very similar values for the surface coverage are observed, being slightly higher for cationic chitosan, which preferentially interacts with the HNT outer surface, wrapping the nanotubes. On the other hand, anionic alginate should mostly be confined within the positively charged HNT cavity. It might also be noted that the obtained Z values for the ionic biopolymers correspond to a "dry" (neglecting hydration water, which, of course, will be there at the real surface layer) polymer layer thickness of ~1.6–1.8 nm, which is a realistic value for dense polymer coverage.

Similar to our previous work on HNT/surfactant hybrids,[33] SANS curves of HNT/biopolymer mixtures were simulated by using a hollow cylinder with a uniform SLD profile (Fig. 3).

According to this model, the scattering intensity can be expressed as

$$I(q) = {}^1N \times P(q, R_i, \Delta R, \sigma, L, SLD_{HNT/Biop}, SLD_s) + I_{bck} \quad (8)$$

where the form factor is $P(q, R_i, \Delta R, \sigma, L, SLD_{HNT/Biop}, SLD_s)$, and R_i, ΔR and L are the geometrical parameters (internal radius, shell thickness and length, respectively), I_{bck} is the incoherent scattered background (evaluated by Porod analysis applied to the larger q range), and $SLD_{HNT/Biop}$ and SLD_s are the scattering length densities of the nanotube shell and solvent, respectively. Namely, we assumed that the biopolymer is included in the shell of the hollow cylinder, while the core is based on pure D_2O. The same assumption was considered for the SANS data analysis of halloysite nanotubes modified with anionic surfactants, which are selectively adsorbed within their cavity.[33] $SLD_{HNT/Biop}$ was estimated on the basis of the composition of the biopolymer coated HNT determined from the Guinier analysis of SANS data in the low q range (Table 2). The $SLD_{HNT/Biop}$ values used for the simulation of the SANS curves of the HNT/biopolymer mixtures are presented in the ESI.† Based on the Schulz–Zimm distribution,[54] a polydispersity (σ) defined as $(\langle\Delta R^2\rangle/\langle\Delta R\rangle^2) - 1$ was considered for the shell thickness. As reported for the simulation of pure HNT from the Matauri Bay deposit,[45] R_i and L were fixed at 15 and 1000 nm, respectively.

Electric birefringence (EBR): the effect of biopolymer adsorption on the HNT rotational mobility

The analysis of EBR results allowed us to investigate the influence of the biopolymer adsorption on the rotational mobility of halloysite nanotubes. As an example, Fig. 4a displays the relaxation of the birefringence signal for the HNT/HPC aqueous mixture (mass ratio = 0.1). It can be noted that the electric field pulse was chosen to be so short that no saturation of the signal took place, but only an initial orientation was imposed.

As observed for the pure HNT[45] and for HNT/surfactant hybrids,[33] a transient birefringence was induced by the electric field applied in the form of a rectangular pulse. This phenomenon is related to the HNT polarizability that causes a partial alignment of the nanotubes. Once the voltage pulse is terminated, the nanotubes are free to reorient and, consequently, the magnitude of the birefringence (Δn) exponentially decreases with time following the equation

$$\Delta n = \Delta n_0 \exp(-t/\tau) \quad (9)$$

where τ is the characteristic relaxation time of the nanotubes, while Δn_0 represents the maximum of the birefringence signal. As an example, the fitting analysis of Δn *vs.* t decay for the HNT/HPC aqueous mixture (mass ratio = 0.1) is reported in the ESI†. Fig. 5 shows the dependence of τ on the biopolymer/HNT mass ratio ($R_{w(Biop/HNT)}$) of the mixtures. The corresponding rotational diffusion coefficient (D_{rot}) reported in the ESI† was calculated as $D_{rot} = (6\tau)^{-1}$.

Open Access Article. Published on 16 2563. Downloaded on 31/1/2569 9:59:45.
This article is licensed under a Creative Commons Attribution 3.0 Unported Licence.

Open Access Article. Published on 16 2563. Downloaded on 31/1/2569 9:59:45.
This article is licensed under a Creative Commons Attribution 3.0 Unported Licence.

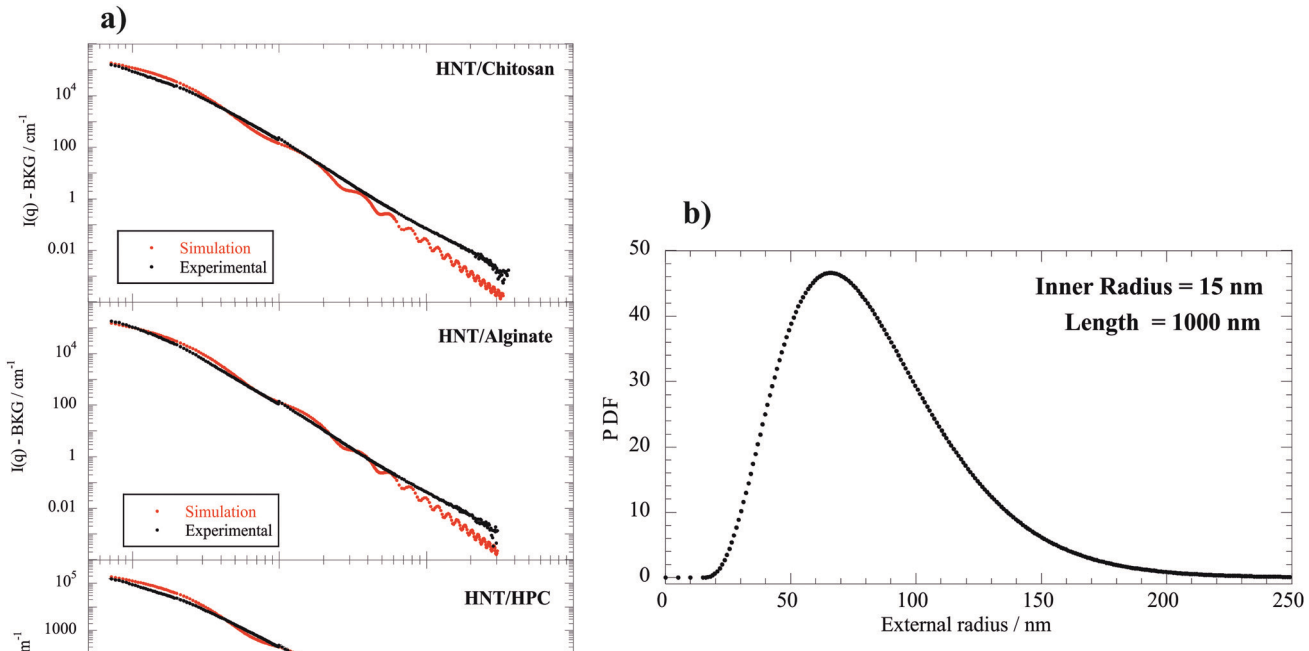

Fig. 3 (a) SANS intensity as a function of q, the magnitude of the scattering vector, after background subtraction for HNT/alginate, HNT/chitosan and HNT/HPC dispersions in D_2O. The best simulation results (red points) were obtained according to a hollow cylinder as model (eqn (8)) with fixed length (1000 nm) and inner radius (15 nm). (b) Schulz–Zimm distribution for the external radius was centered at 65 nm. The incoherent scattered background was evaluated by Porod analysis applied to the larger q range.

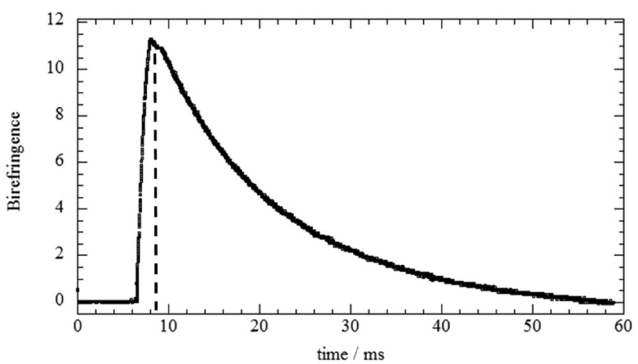

Fig. 4 Transient electric-field-induced birefringence signal for aqueous dispersion with a HPC/HNT mass ratio of 0.1. The HNT concentration was 0.15 g dm^{-3}. The experiments were conducted using rectangular pulses (the applied electric field and the pulse length were fixed at 1.25×10^5 V m^{-1} and 2.5 ms, respectively). The dashed line represents the time point where the electric field was switched off.

As a general result, the presence of the biopolymer induced a τ enhancement indicating that the rotational mobility of the nanotubes was reduced. This effect can be attributed to the biopolymer adsorption onto the halloysite surfaces. In particular, τ *vs.* $R_{w(Biop/HNT)}$ plots exhibited increasing trends for $R_{w(Biop/HNT)} \leq 0.3$, while further addition of the biopolymer did not affect the relaxation time of the nanotubes. This indicates that here the attachment of the biopolymer is effectively saturated. In this regard, it should be noted that the reduction of the HNT rotational mobility cannot be simply attributed to the increase of mass upon adsorption because the amount of the biopolymer bound to the halloysite surfaces is less than 2% for all the investigated systems (Table 2). It should be noted that the presence of biopolymer causes a slow enhancement of the viscosity, which could contribute to the reduction of the HNT rotational mobility. However, this effect is negligible because the biopolymer concentration range is within a dilute regime (up to *ca.* 0.12 wt%). As an example, a relative D_{rot} variation of only 7% is expected for the aqueous HPC/HNT mixture (with concentrations of 1 and 0.1 wt% for halloysite and polymer, respectively), because its intrinsic viscosity is 1.078, as reported in our previous paper.[36] In addition, the influence of the polymer concentration on D_{rot} would be more important if the solvent viscosity significantly affected the HNT rotational mobility. Accordingly, overlapping and/or bridging of the polymer-coated nanotubes could be expected for the investigated mixtures. Compared to non-ionic HPC, ionic biopolymers induced stronger effects on the HNT rotational mobility due to the electrostatic interactions. The selective

 This journal is © the Owner Societies 2020

Open Access Article. Published on 16 2563. Downloaded on 31/1/2569 9:59:45.
This article is licensed under a Creative Commons Attribution 3.0 Unported Licence.

interactions of the polyelectrolytes with the charged HNT surfaces affected their influence on the rotational diffusion of the nanotubes. The effect of chitosan on the HNT rotational mobility is stronger with respect to that of alginate, which is mostly confined to the positively charged clay lumen. These results could indicate that chitosan is bound at the outside surface interconnecting different HNTs, thus substantially slowing down their rotation.

In addition, D_{rot} values allowed us to determine the length of the nanotubes in the biopolymer/halloysite mixtures by using Broersma theory, which is valid for rigid rods with length/diameter ratios between 2 and 30. This approach was successfully employed for halloysite nanotubes modified with anionic surfactants.[33] Details on the calculation of the HNT length using Broersma theory are presented in the ESI.† We estimated that the HNT length in water is 809 ± 7 nm. As a general result, the presence of biopolymers induced an increase of the halloysite length (see ESI†). In particular, the chitosan adsorption generated the strongest effect on the HNT length, which reached the largest value of 1228 ± 11 nm for the biopolymer/HNT mass ratio of 0.67. According to the EBR results, we estimated the overlap concentration for HNTs by assuming a simple cubic model where the contact distance corresponds to the length of the nanotubes. Specifically, the critical volume fraction (ϕ^*) for the HNT overlapping was calculated as $\pi R^2/L^2$. As concerns pure HNTs, we determined that the overlap concentration is *ca.* 500 times higher with respect to the concentration of the investigated dispersion, confirming that the EBR results reflect the free rotation of the nanotubes. We observed that the overlap concentrations for biopolymer-coated nanotubes are *ca.* 2 orders higher with respect to the concentration of the investigated mixtures. Therefore, the influence of the biopolymer adsorption on the HNT rotational mobility can be explored by the EBR data.

Fluorescence correlation spectroscopy (FCS): the influence of the adsorption onto the HNT surfaces on biopolymer dynamic behavior in aqueous medium

The influence of the HNT/biopolymer electrostatic interactions on the dynamic behaviour in water of the biopolyelectrolytes was explored by FCS studies. Biopolymers were fluorescently labelled with proper probes, such as FITC and DTAF for chitosan and alginate, respectively. Fig. 6 shows the effect of the HNT addition on the correlation function of the FITC/chitosan aqueous solution.

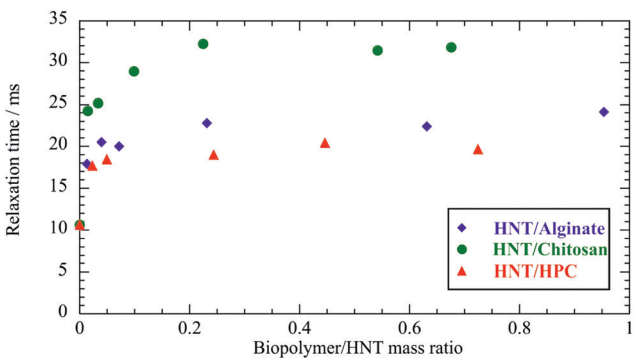

Fig. 5 Relaxation time determined by the fitting of the EBR data as a function of the biopolymer/HNT mass ratio at a HNT concentration of 0.15 g dm^{-3} (SANS and FCS experiments were done at 0.1).

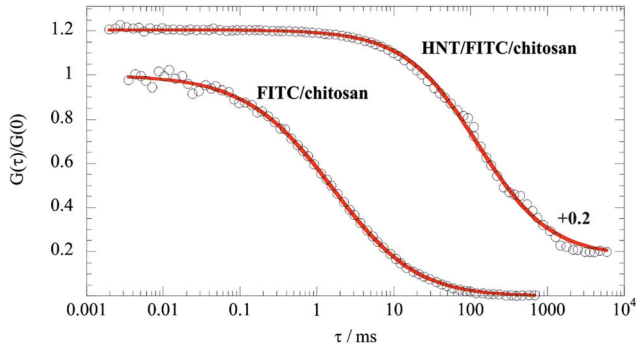

Fig. 6 Normalized FCS decay curves for FITC/chitosan and HNT/FITC/chitosan mixtures in water. The concentration of the labeled chitosan (FITC/chitosan) was set at 0.05 mg dm^{-3}, while the overall concentration of chitosan was fixed at 5 g dm^{-3}. Accordingly, the labelled chitosan/HNT mass ratio was 10^{-4} and the chitosan/HNT mass ratio was 0.1. Red lines represent the fitting according to the pure diffusion model (eqn (10)). The FCS curve for HNT/FITC/chitosan was arbitrarily shifted along the *y*-axis by adding a constant 0.2 to the experimental data.

According to the adsorption process, a significant reduction of the biopolymer mobility was detected in the presence of HNT. As evidenced by Fig. 6, the correlation functions of both FITC/chitosan and HNT/FITC/chitosan systems were successfully described by the stretched model expressed by the following equation[55]

$$G(\tau) = G(0)\cdot\left[\left(1+\left(\frac{T}{1-T}\right)\right)\exp(-\tau/\tau_T)\right]\cdot\left(1+\left(\frac{\tau}{\tau_c}\right)^{\alpha}\right)^{-1}\left(1+\frac{1}{S^2}\left(\frac{\tau}{\tau_c}\right)^{\alpha}\right)^{-0.5} \quad (10)$$

where T is the fraction of the molecules in the triplet state, α is the stretched parameter and τ_T is their relaxation time. S is given by the anisotropy (ratio of the vertical and lateral extensions), while τ_c and $G(0)$ are the intercept and the decay time, respectively. As reported in the literature,[56] the contribution of the triplet state cannot be neglected for DTAF molecules, while we did so for FITC.

It should be noted that the pure diffusion model was successfully employed for the FCS data analysis of HNT/surfactant hybrids containing Nile red.[33] Table 3 reports the fitting parameters ($G(0)$ and τ_c) for FITC/chitosan and HNT/FITC/chitosan (α values were 0.770 ± 0.011 and 0.904 ± 0.015, respectively).

In addition, we calculated the diffusion coefficient (D) as

$$D = \omega_0^2/4\tau_c \quad (11)$$

where ω_0 is the lateral extension (590 nm) of the confocal volume.

The decay of FITC/chitosan reflects the dynamic behavior of the polymer, confirming that the fluorescent probe was successfully attached to the chitosan molecule. It is noteworthy that the diffusion coefficient of the HNT/FITC/chitosan mixture is much

Table 3 Intercept and the decay time (with the corresponding diffusion coefficient and hydrodynamic radius) obtained from the fitting analysis of FCS curves. Pure diffusion and triplet state models were employed

	Fitting model	$G(0)$	τ_c/ms	$D/\mu m^2\ s^{-1}$	R_h/nm
FITC/chitosan	Pure diffusion	0.0943 ± 0.0003	1.62 ± 0.03	53.6 ± 1.0	4.56 ± 0.09
HNT/FITC/chitosan	Pure diffusion	0.0782 ± 0.0004	54.8 ± 1.6	1.59 ± 0.05	154 ± 4
DTAF/alginate	Triplet state	0.119 ± 0.003	1.80 ± 0.29	48 ± 8	5.1 ± 0.8
HNT/DTAF/alginate	Triplet state	0.078 ± 0.007	3.5 ± 1.0	24 ± 7	10 ± 2

Open Access Article. Published on 16 2563. Downloaded on 31/1/2569 9:59:45.
This article is licensed under a Creative Commons Attribution 3.0 Unported Licence.

larger (*ca.* 50 times) with respect to that of the pure labeled polymer, which proves the strong binding of chitosan. Table 3 compares the corresponding hydrodynamic radius (R_h) calculated by using the Stoke–Einstein equation. In contrast, the presence of HNT led only to a small reduction of mobility of DTAF/alginate (Fig. 7), which indicates here only a rather weak extent of binding.

The ESI† reports the fitting parameters obtained by the fitting through the triplet state model[56] of FCS curves for DTAF/alginate and HNT/DTAF/alginate suspensions. The presence of HNT induced a reduction by a factor of 2 for the diffusion coefficient of the DTAF/alginate. Based on the FCS results, we can assert that dynamic behavior in water of both biopolyelectrolytes decreases as a consequence of their adsorption onto HNT surfaces. This effect is much stronger for cationic chitosan, which is wrapped onto the nanotubes. We can assume that the D values for HNT/labeled polymers are given by two contributions: (1) the fast diffusion process (D_{fast}), which is related to the unbound polymer; (2) the slow diffusion (D_{slow}) due to the diffusion of the polymer adsorbed onto HNT surfaces. Based on the SANS data analysis (Table 2), only *ca.* 2 wt% of both chitosan and alginate are bound onto HNT. Therefore, the fast process should be predominant in the experimental diffusion coefficient. This consideration is valid for HNT/DTAF/alginate, while the much slower diffusion of HNT/FITC/chitosan could indicate that the biopolymer becomes immobilized by bridging different HNTs. In conclusion, FCS findings agree with the EBR data, which evidenced that chitosan adsorption induced the most significant reduction of the HNT rotational diffusion coefficient. Based on these results, we can argue that bridging between chitosan-coated nanotubes can be hypothesized.

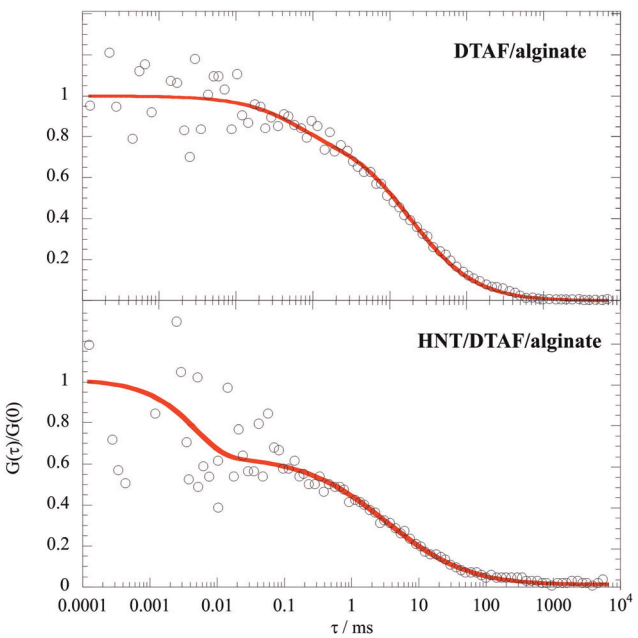

Fig. 7 Normalized FCS decay curves for DTAF/alginate and HNT/DTAF/alginate mixtures in water. The concentration of DTAF/alginate was set at 0.1 mg dm^{-3}, while the overall concentration of alginate was fixed at 10 g dm^{-3}. Accordingly, the labelled alginate/HNT mass ratio was 10^{-4} and the mass ratio between the overall alginate and HNT was 0.1. Red lines represent the fitting according to the triplet state model.[56]

Conclusions

We investigated the structural behavior of aqueous mixtures composed of halloysite nanotubes (HNTs) and differently charged biopolymers, such as cationic chitosan, anionic alginate and non-ionic hydroxypropylcellulose. The simulation of SANS curves by a hollow cylinder model evidenced that the biopolymer coated nanotubes possesses similar geometrical features (in terms of sizes and polydispersity) as those previously observed for pure HNT. SANS data at low and intermediate q were successfully analyzed by the Guinier approach for rod-like objects. In addition, the SANS analysis showed that charged biopolymers exhibit larger adsorption efficiencies that can be attributed to the stronger electrostatic interactions. In agreement, EBR results showed that the decrease of the HNT rotational mobility is more affected and reduced for halloysite/ionic biopolymer mixtures. In this respect, chitosan caused a somewhat stronger alteration of the halloysite rotational mobility because of the HNT wrapping driven by the attractive forces between the positively charged biopolymer and the halloysite external surface, which is positively charged. The analysis of FCS curves evidenced that the adsorption process decreases the aqueous diffusion coefficients of both polyelectrolytes. The stronger effect is observed for the HNT/chitosan mixture, which showed a reduction by *ca.* 50% compared to that of the pure biopolymer as a consequence of the wrapping process. In conclusion, a systematic correlation between the structure of the HNT/biopolymer hybrid and the structure of the biopolymer was demonstrated by the investigation of aqueous mixtures by applying a comprehensive set of characterisation techniques (SANS, EBR, and FCS) to these composites.

Conflicts of interest

The authors have no conflicts of interest to declare.

This journal is © the Owner Societies 2020

Open Access Article. Published on 16 2563. Downloaded on 31/1/2569 9:59:45.
This article is licensed under a Creative Commons Attribution 3.0 Unported Licence.

Acknowledgements

The work was financially supported by Progetto di ricerca e sviluppo ''AGM for CuHe'' (ARS01_00697), DAAD (Deutscher Akademischer Austauschdienst, Research Grants for Doctoral Candidates and Young Academics and Scientists 2016/2017 – funding 57210260) and University of Palermo. ILL is thanked for granting SANS beamtime. The support from the PSCM (Partnership for Soft Condensed Matter) at the ILL is acknowledged. The authors thank Miriam Simon for her support in FCS experiments.

References

1 M. Du, B. Guo, Y. Lei, M. Liu and D. Jia, Carboxylated butadiene–styrene rubber/halloysite nanotube nanocomposites: Interfacial interaction and performance, *Polymer*, 2008, **49**, 4871–4876.

2 M. Du, B. Guo and D. Jia, Newly emerging applications of halloysite nanotubes: a review, *Polym. Int.*, 2010, **59**, 574–582.

3 C. H. Zhou, An overview on strategies towards clay-based designer catalysts for green and sustainable catalysis, *Appl. Clay Sci.*, 2011, **53**, 87–96.

4 S. Sadjadi, T. Hosseinnejad, M. Malmir and M. M. Heravi, Cu@furfural imine-decorated halloysite as an efficient heterogeneous catalyst for promoting ultrasonic-assisted A3 and KA2 coupling reactions: a combination of experimental and computational study, *New J. Chem.*, 2017, **41**, 13935–13951.

5 S. Sadjadi, M. M. Heravi and M. Malmir, Pd@HNTs-CDNS-g-C_3N_4: A novel heterogeneous catalyst for promoting ligand and copper-free Sonogashira and Heck coupling reactions, benefits from halloysite and cyclodextrin chemistry and g-C_3N_4 contribution to suppress Pd leaching, *Carbohydr. Polym.*, 2018, **186**, 25–34.

6 Y. Liu, J. Zhang, H. Guan, Y. Zhao, J.-H. Yang and B. Zhang, Preparation of bimetallic Cu–Co nanocatalysts on poly(diallyldimethylammonium chloride) functionalized halloysite nanotubes for hydrolytic dehydrogenation of ammonia borane, *Appl. Surf. Sci.*, 2018, **427**, 106–113.

7 Y. Zhao, W. Kong, Z. Jin, Y. Fu, W. Wang, Y. Zhang, J. Liu and B. Zhang, Storing solar energy within Ag-Paraffin@Halloysite microspheres as a novel self-heating catalyst, *Appl. Energy*, 2018, **222**, 180–188.

8 Y. Lvov, W. Wang, L. Zhang and R. Fakhrullin, Halloysite Clay Nanotubes for Loading and Sustained Release of Functional Compounds, *Adv. Mater.*, 2016, **28**, 1227–1250.

9 F. Liu, L. Bai, H. Zhang, H. Song, L. Hu, Y. Wu and X. Ba, Smart H_2O_2-Responsive Drug Delivery System Made by Halloysite Nanotubes and Carbohydrate Polymers, *ACS Appl. Mater. Interfaces*, 2017, **9**, 31626–31633.

10 A. P. F. Monteiro, L. D. Caminhas, J. D. Ardisson, R. Paniago, M. E. Cortés and R. D. Sinisterra, Magnetic nanoparticles coated with cyclodextrins and citrate for irinotecan delivery, *Carbohydr. Polym.*, 2017, **163**, 1–9.

11 Y. Stetsyshyn, J. Zemla, O. Zolobko, K. Fornal, A. Budkowski, A. Kostruba, V. Donchak, K. Harhay, K. Awsiuk, J. Rysz, A. Bernasik and S. Voronov, Temperature and pH dual-responsive coatings of oligoperoxide-*graft*-poly(*N*-isopropylacrylamide): Wettability, morphology, and protein adsorption, *J. Colloid Interface Sci.*, 2012, **387**, 95–105.

12 M. Liu, C. Wu, Y. Jiao, S. Xiong and C. Zhou, Chitosan-halloysite nanotubes nanocomposite scaffolds for tissue engineering, *J. Mater. Chem. B*, 2013, **1**, 2078–2089.

13 L. Lisuzzo, G. Cavallaro, P. Pasbakhsh, S. Milioto and G. Lazzara, Why does vacuum drive to the loading of halloysite nanotubes? The key role of water confinement, *J. Colloid Interface Sci.*, 2019, **547**, 361–369.

14 C. Cheng, Y. Gao, W. Song, Q. Zhao, H. Zhang and H. Zhang, Halloysite nanotube-based H_2O_2-responsive drug delivery system with a turn on effect on fluorescence for real-time monitoring, *Chem. Eng. J.*, 2020, **380**, 122474.

15 T. Sakthivel, D. L. Reid, I. Goldstein, L. Hench and S. Seal, Hydrophobic High Surface Area Zeolites Derived from Fly Ash for Oil Spill Remediation, *Environ. Sci. Technol.*, 2013, **47**, 5843–5850.

16 A. Panchal, L. T. Swientoniewski, M. Omarova, T. Yu, D. Zhang, D. A. Blake, V. John and Y. M. Lvov, Bacterial proliferation on clay nanotube Pickering emulsions for oil spill bioremediation, *Colloids Surf., B*, 2018, **164**, 27–33.

17 L. Qin, Y. Zhao, J. Liu, J. Hou, Y. Zhang, J. Wang, J. Zhu, B. Zhang, Y. Lvov and B. Van der Bruggen, Oriented Clay Nanotube Membrane Assembled on Microporous Polymeric Substrates, *ACS Appl. Mater. Interfaces*, 2016, **8**, 34914–34923.

18 P. R. Maddigpu, B. Sawant, S. Wanjari, M. D. Goel, D. Vione, R. S. Dhodapkar and S. Rayalu, Carbon nanoparticles for solar disinfection of water, *J. Hazard. Mater.*, 2018, **343**, 157–165.

19 J. Lee, J. Ko, J. Ryu, J. Shin, H. Kim and D. Sohn, Catechol grafted silica particles for enhanced adhesion to metal by coordinate bond, *Colloids Surf., A*, 2016, **511**, 55–63.

20 G. Lazzara, G. Cavallaro, A. Panchal, R. Fakhrullin, A. Stavitskaya, V. Vinokurov and Y. Lvov, An assembly of organic-inorganic composites using halloysite clay nanotubes, *Curr. Opin. Colloid Interface Sci.*, 2018, **35**, 42–50.

21 H. Kong, W. Li, C. Gao, D. Yan, Y. Jin, D. R. M. Walton and H. W. Kroto, Poly(*N*-isopropylacrylamide)-Coated Carbon Nanotubes: Temperature-Sensitive Molecular Nanohybrids in Water, *Macromolecules*, 2004, **37**, 6683–6686.

22 S. Kalay, Y. Stetsyshyn, V. Lobaz, K. Harhay, H. Ohar and M. Çulha, Water-dispersed thermo-responsive boron nitride nanotubes: synthesis and properties, *Nanotechnology*, 2016, **27**, 035703.

23 G. Cavallaro, G. Lazzara, L. Lisuzzo, S. Milioto and F. Parisi, Selective adsorption of oppositely charged PNIPAAM on halloysite surfaces: A route to thermo-responsive nanocarriers, *Nanotechnology*, 2018, **29**, 325702.

24 G. Wang, D. Maciel, Y. Wu, J. Rodrigues, X. Shi, Y. Yuan, C. Liu, H. Tomás and Y. Li, Amphiphilic Polymer-Mediated Formation of LAPONITE-Based Nanohybrids with Robust Stability and pH Sensitivity for Anticancer Drug Delivery, *ACS Appl. Mater. Interfaces*, 2014, **6**, 16687–16695.

25 J.-L. Wu, C.-Q. Wang, R.-X. Zhuo and S.-X. Cheng, Multi-drug delivery system based on alginate/calcium carbonate

Open Access Article. Published on 16 2563. Downloaded on 31/1/2569 9:59:45.
This article is licensed under a Creative Commons Attribution 3.0 Unported Licence.

hybrid nanoparticles for combination chemotherapy, *Colloids Surf., B*, 2014, **123**, 498–505.
26 M. Boissière, J. Allouche, C. Chanéac, R. Brayner, J.-M. Devoisselle, J. Livage and T. Coradin, Potentialities of silica/alginate nanoparticles as Hybrid Magnetic Carriers, *New Trends Drug Deliv. Syst.*, 2007, **344**, 128–134.
27 D. A. Prishchenko, E. V. Zenkov, V. V. Mazurenko, R. F. Fakhrullin, Y. M. Lvov and V. G. Mazurenko, Molecular dynamics of the halloysite nanotubes, *Phys. Chem. Chem. Phys.*, 2018, **20**, 5841–5849.
28 H. Zhang, T. Ren, Y. Ji, L. Han, Y. Wu, H. Song, L. Bai and X. Ba, Selective Modification of Halloysite Nanotubes with 1-Pyrenylboronic Acid: A Novel Fluorescence Probe with Highly Selective and Sensitive Response to Hyperoxide, *ACS Appl. Mater. Interfaces*, 2015, **7**, 23805–23811.
29 Z. Luo, H. Song, X. Feng, M. Run, H. Cui, L. Wu, J. Gao and Z. Wang, Liquid Crystalline Phase Behavior and Sol–Gel Transition in Aqueous Halloysite Nanotube Dispersions, *Langmuir*, 2013, **29**, 12358–12366.
30 Z. Luo, A. Wang, C. Wang, W. Qin, N. Zhao, H. Song and J. Gao, Liquid crystalline phase behavior and fiber spinning of cellulose/ionic liquid/halloysite nanotubes dispersions, *J. Mater. Chem. A*, 2014, **2**, 7327–7336.
31 G. Cavallaro, G. Lazzara, S. Milioto and F. Parisi, Hydrophobically Modified Halloysite Nanotubes as Reverse Micelles for Water-in-Oil Emulsion, *Langmuir*, 2015, **31**, 7472–7478.
32 G. Cavallaro, G. Lazzara, S. Milioto, F. Parisi, V. Evtugyn, E. Rozhina and R. Fakhrullin, Nanohydrogel Formation within the Halloysite Lumen for Triggered and Sustained Release, *ACS Appl. Mater. Interfaces*, 2018, **10**, 8265–8273.
33 G. Cavallaro, I. Grillo, M. Gradzielski and G. Lazzara, Structure of Hybrid Materials Based on Halloysite Nanotubes Filled with Anionic Surfactants, *J. Phys. Chem. C*, 2016, **120**, 13492–13502.
34 G. Cavallaro, G. Lazzara, S. Milioto, F. Parisi and V. Sanzillo, Modified halloysite nanotubes: Nanoarchitectures for enhancing the capture of oils from vapor and liquid phases, *ACS Appl. Mater. Interfaces*, 2014, **6**, 606–612.
35 J. Tully, R. Yendluri and Y. Lvov, Halloysite Clay Nanotubes for Enzyme Immobilization, *Biomacromolecules*, 2016, **17**, 615–621.
36 V. Bertolino, G. Cavallaro, G. Lazzara, S. Milioto and F. Parisi, Biopolymer-Targeted Adsorption onto Halloysite Nanotubes in Aqueous Media, *Langmuir*, 2017, **33**, 3317–3323.
37 P. R. Chang, Y. Xie, D. Wu and X. Ma, Amylose wrapped halloysite nanotubes, *Carbohydr. Polym.*, 2011, **84**, 1426–1429.
38 M. Liu, Z. Huo, T. Liu, Y. Shen, R. He and C. Zhou, Self-Assembling Halloysite Nanotubes into Concentric Ring Patterns in a Sphere-on-Flat Geometry, *Langmuir*, 2017, **33**, 3088–3098.
39 Y. Zhao, G. Cavallaro and Y. Lvov, Orientation of charged clay nanotubes in evaporating droplet meniscus, *J. Colloid Interface Sci.*, 2015, **440**, 68–77.
40 H. Li, X. Zhu, J. Xu, W. Peng, S. Zhong and Y. Wang, The combination of adsorption by functionalized halloysite nanotubes and encapsulation by polyelectrolyte coatings for sustained drug delivery, *RSC Adv.*, 2016, **6**, 54463–54470.
41 L. Lisuzzo, G. Cavallaro, S. Milioto and G. Lazzara, Layered composite based on halloysite and natural polymers: a carrier for the pH controlled release of drugs, *New J. Chem.*, 2019, **43**, 10887–10893.
42 G. Lazzara, G. Cavallaro, L. Chiappisi and I. Grillo, *Inst. Laue-Langevin ILL*, 2016, DOI: 10.5291/ILL-DATA.9-12-473.
43 D. Richard, M. Ferrand and G. J. Kearley, *Anal. Vis. Neutron-Scatt. Data*, 1996, 33–39.
44 I. Bressler, J. Kohlbrecher and A. F. Thünemann, SASfit: a tool for small-angle scattering data analysis using a library of analytical expressions, *J. Appl. Crystallogr.*, 2015, **48**, 1587–1598.
45 G. Cavallaro, L. Chiappisi, P. Pasbakhsh, M. Gradzielski and G. Lazzara, A structural comparison of halloysite nanotubes of different origin by Small-Angle Neutron Scattering (SANS) and Electric Birefringence, *Appl. Clay Sci.*, 2018, **160**, 71–80.
46 P.-O. Gendron, F. Avaltroni and K. J. Wilkinson, Diffusion Coefficients of Several Rhodamine Derivatives as Determined by Pulsed Field Gradient–Nuclear Magnetic Resonance and Fluorescence Correlation Spectroscopy, *J. Fluoresc.*, 2008, **18**, 1093–1101.
47 A. R. Mackie, A. Macierzanka, K. Aarak, N. M. Rigby, R. Parker, G. A. Channell, S. E. Harding and B. H. Bajka, Sodium alginate decreases the permeability of intestinal mucus, *Food Hydrocolloids*, 2016, **52**, 749–755.
48 A. Mackie, B. Bajka and N. Rigby, Roles for dietary fibre in the upper GI tract: The importance of viscosity, *Food Res. Int.*, 2016, **88**, 234–238.
49 P. Tallury, S. Kar, S. Bamrungsap, Y.-F. Huang, W. Tan and S. Santra, Ultra-small water-dispersible fluorescent chitosan nanoparticles: synthesis, characterization and specific targeting, *Chem. Commun.*, 2009, 2347–2349.
50 O. Glatter and O. Kratky, *Small angle X-ray scattering*, Academic Press, New York, 1982.
51 B. Hammouda, Analysis of the Beaucage model, *J. Appl. Crystallogr.*, 2010, **43**, 1474–1478.
52 H. Brumberger, *Modern Aspects of Small-Angle Scattering*, Kluver Academic, Dordrecht, 1995.
53 R. Joksimovic, S. Prévost, R. Schweins, M.-S. Appavou and M. Gradzielski, Interactions of silica nanoparticles with poly(ethylene oxide) and poly(acrylic acid): Effect of the polymer molecular weight and of the surface charge, *J. Colloid Interface Sci.*, 2013, **394**, 85–93.
54 B. H. Zimm, The Scattering of Light and the Radial Distribution Function of High Polymer Solutions, *J. Chem. Phys.*, 1948, **16**, 1093–1099.
55 T. Kihara, J. Ito and J. Miyake, Measurement of Biomolecular Diffusion in Extracellular Matrix Condensed by Fibroblasts Using Fluorescence Correlation Spectroscopy, *PLoS One*, 2013, **8**, e82382.
56 I. Hoffmann, M. Simon, B. Farago, R. Schweins, P. Falus, O. Holderer and M. Gradzielski, Structure and dynamics of polyelectrolyte surfactant mixtures under conditions of surfactant excess, *J. Chem. Phys.*, 2016, **145**, 124901.